

# Synchronization transition of heterogeneously coupled oscillators on scale-free networks

E. Oh<sup>1</sup>, D.-S. Lee<sup>2</sup>, B. Kahng<sup>1,3</sup> and D. Kim<sup>1</sup>

<sup>1</sup> CTP & FPRD, School of Physics and Astronomy, Seoul National University, Seoul 151-747, Korea

<sup>2</sup> Theoretische Physik, Universität des Saarlandes, 66041 Saarbrücken, Germany

<sup>3</sup> Center for Nonlinear Studies, Los Alamos National Laboratory, Los Alamos, NM 87545

(Dated: July 20, 2018)

We investigate the synchronization transition of the modified Kuramoto model where the oscillators form a scale-free network with degree exponent  $\lambda$ . An oscillator of degree  $k_i$  is coupled to its neighboring oscillators with asymmetric and degree-dependent coupling in the form of  $Jk_i^{\eta-1}$ . By invoking the mean-field approach, we determine the synchronization transition point  $J_c$ , which is zero (finite) when  $\eta > \lambda - 2$  ( $\eta < \lambda - 2$ ). We find eight different synchronization transition behaviors depending on the values of  $\eta$  and  $\lambda$ , and derive the critical exponents associated with the order parameter and the finite-size scaling in each case. The synchronization transition is also studied from the perspective of cluster formation of synchronized vertices. The cluster-size distribution and the largest cluster size as a function of the system size are derived for each case using the generating function technique. Our analytic results are confirmed by numerical simulations.

PACS numbers: 89.75.Hc, 05.45.Xt, 05.70.Fh

## I. INTRODUCTION

Synchronization of oscillations is one of the fundamental nonlinear phenomena in biology, physics, chemistry, communication science, and many other branches of science and engineering [1]. Recently, the dynamics of synchronization of oscillators located at each vertex in complex networks has attracted much attentions. That is because the small-world feature of complex networks is closely related to their synchronizability. By the small-world feature, we mean that the average separation  $\langle d \rangle$  between a pair of vertices scales at most  $\langle d \rangle \sim \log N$ , where  $N$  is the number of vertices in the system. It was shown that a small-world network model introduced by Watts and Strogatz [2] is more synchronizable than regular lattice [3]. However, such feature is not observed in scale-free (SF) networks. SF networks are the networks that exhibit a power-law degree distribution  $P_d(k) \sim k^{-\lambda}$  and degree  $k$  is the number of edges connected to a given vertex [4]. In SF networks, the heterogeneity in the degree distribution suppresses their synchronizability [5]. Thus, it was desired to introduce a new dynamic model that prompts SF networks to be more synchronizable.

The dynamics of synchronization is described by various forms of coupled equations. A linearly coupled model is probably the simplest one. In the model,  $N$  oscillators are coupled when they are connected via edges. Coupling constant is normally symmetric; however, it is not necessarily symmetric to achieve a better synchronizability. This case can happen in SF networks: It was shown recently [6] that the synchronizability becomes maximum when information flow diffuses and reaches a uniform stationary state over the entire system. Here, the mapping from synchronization dynamics to information flow can be naturally introduced, because the linearly coupled equation is nothing but the diffusion equation. It was shown that the uniform-stationary state can be

reached by introducing asymmetric and weighted coupling strength between a pair of vertices or oscillators.

To be specific, the dynamic model with the asymmetric coupling strength is written as

$$\frac{d\phi_i}{dt} = f(\phi_i) - \frac{J}{k_i^{1-\eta}} \sum_{j=1}^N a_{ij} (h(\phi_i) - h(\phi_j)) \quad (1)$$

for  $i = 1, \dots, N$ . Here,  $\phi_i$  is the phase of an oscillator located at vertex  $i$ ,  $f(\phi)$  describes the dynamics of an individual oscillator,  $J$  is the overall coupling strength.  $k_i$  is the degree of vertex  $i$ , and  $a_{ij}$  is an element of the adjacent matrix, which is 1 if vertices  $i$  and  $j$  are connected and 0 otherwise.  $h(\phi_i)$  is the output function and take a form of  $h(\phi_i) = \phi_i$  for the linear case. It is noteworthy that the coupling strength of Eq. (1) is asymmetric and weighted due to the factor  $1/k_i^{1-\eta}$  unless  $\eta = 1$ . When  $\eta > 0$ , vertices with large degree can influence other vertices significantly on regulating phases due to their large numbers of connections; on the other hand, when  $\eta < 0$ , the influence is reduced. It was found [6] that the system is most synchronizable when  $\eta = 0$ , irrespective of the value of the degree exponent of a given SF network.

In this paper, we study the pattern of synchronization transition for a modified Kuramoto model [7], which is similarly modified with the asymmetric and weighted coupling strength as

$$\frac{d\phi_i}{dt} = \omega_i - \frac{J}{k_i^{1-\eta}} \sum_{j=1}^N a_{ij} \sin(\phi_i - \phi_j). \quad (2)$$

The oscillators are located at each vertex  $i = 1, \dots, N$  of a SF network with degree exponent  $\lambda$ . Here,  $\omega_i$  is the natural frequency of the  $i$ th oscillator selected from the Gaussian distribution  $g(\omega) = e^{-\omega^2/2}/\sqrt{2\pi}$ . We find that the modified Kuramoto dynamic model displays a

very complex and rich behaviors in the space of the two tunable parameters ( $\eta, \lambda$ ).

The synchronization transition from a desynchronized to a synchronized state occurs at the critical point  $J_c$ . For small  $J \ll J_c$ , the coupling strength is so weak that an individual vertex maintains its own phase different from others; therefore, the entire system is desynchronized. As the coupling strength  $J$  increases, a cluster of vertices is more likely to be coupled, to be in a common or almost the same phase, and thus forms a cluster of synchrony. Size of such clusters becomes diverse as the coupling strength  $J$  increases. At the critical point  $J_c$ , the system reaches a self-organized state, and the cluster-size distribution follows a power law,

$$n(s) \sim s^{-\tau-1} \quad (3)$$

in the thermodynamic limit. For  $J \gg J_c$ , the power-law behavior no longer holds and the entire system is synchronized.

The order parameter of the synchronization transition is defined as

$$r e^{i\theta} = \frac{1}{N} \sum_{i=1}^N e^{i\phi_i}. \quad (4)$$

In the synchronized state, the phases  $\phi_i$  of each vertex are narrowly distributed around an average phase  $\theta$ . The amplitude  $r$  of the order parameter has a finite value; on the other hand,  $r \approx 0$  in the desynchronized state. Thus, the exponent  $\beta$  associated with the order parameter is defined via the relation,

$$r \sim \Delta^\beta, \quad (5)$$

where  $\Delta = (J - J_c)/J_c$ . In finite-size systems, the order parameter is described in terms of a scaling function as

$$r \sim N^{-\beta/\mu} \psi(\Delta N^{1/\mu}). \quad (6)$$

In the recent works [8, 9], the nature of the transitions and the finite-size scalings have been studied for the case of  $\eta = 1$ . In this work, we determine the order parameter and the size distribution of synchronized clusters for general  $\eta$  using the mean-field approach and the generating function technique. Moreover, we construct a finite-size scaling function for the order parameter, and determine the exponent  $\mu$ . Even for a simple extension of  $\eta \neq 1$ , we find that the obtained result is very rich. There exist eight distinct transition behaviors depending on the values of  $\eta$  and  $\lambda$ . Therefore, the result can be helpful in understanding diverse dynamic phenomena arising on SF networks.

The paper is organized as follows: In Sec. II, we first introduce and apply the mean-field approach to the dynamic equation (2). We construct a self-consistent equation for a local field and determine the order parameter. Next, the critical point is determined and the behavior of the order parameter near the critical point is obtained

in Sec. III. The size distribution of synchronized clusters and the largest cluster size at the critical point are solved in Secs. IV and V, respectively. The finite-size scaling analysis for the order parameter is performed and the results are checked numerically in Sec. VI. Summary and discussion follow in Sec. VII.

## II. ORDER PARAMETER EQUATION

In this section, we analyze the modified Kuramoto equation (2) in the framework of the mean-field approach by constructing a self-consistent equation for a local field. To proceed, we define  $\bar{r}_i$  and  $\bar{\theta}_i$  as the amplitude and phase of the local field at vertex  $i$ , respectively, via

$$\bar{r}_i e^{i\bar{\theta}_i} = \frac{1}{k_i} \sum_{j=1}^N a_{ij} e^{i\phi_j}. \quad (7)$$

Then, Eq. (2) is rewritten in terms of the local field as

$$\frac{d\phi_i}{dt} = \omega_i - J \bar{r}_i k_i^\eta \sin(\phi_i - \bar{\theta}_i). \quad (8)$$

Once the amplitude  $\bar{r}_i$  and the phase  $\bar{\theta}_i$  of the local field are determined, one can solve Eq. (8) easily. The local field  $\bar{r}_i$  is determined in a self-consistent manner.

We consider the probability density  $\rho_i^{(s)}(\phi|\omega)d\phi$  that the phase of an oscillator  $i$  with natural frequency  $\omega$  lies between  $\phi$  and  $\phi + d\phi$  in the steady state [10]. Using a previous result [10] that  $\rho_i^{(s)}(\phi|\omega)d\phi$  is inversely proportional to the speed of  $\phi$ , one can obtain that

$$\rho_i^{(s)}(\phi|\omega) = \begin{cases} \delta \left[ \phi - \bar{\theta}_i - \sin^{-1} \left( \frac{\omega}{\omega_{*,i}} \right) \right] & \text{if } |\omega| \leq \omega_{*,i}, \\ \frac{\sqrt{\omega^2 - \omega_{*,i}^2}}{2\pi |\omega - \omega_{*,i} \sin(\phi - \bar{\theta}_i)|} & \text{otherwise,} \end{cases} \quad (9)$$

where  $\omega_{*,i} = J \bar{r}_i k_i^\eta$ . This result implies that an oscillator  $i$  with natural frequency  $\omega$  has its phase that is locked at  $\phi = \bar{\theta}_i + \sin^{-1}(\omega/\omega_{*,i})$  and  $d\phi_i/dt = 0$  if  $|\omega| \leq \omega_{*,i}$ . Otherwise, its phase drifts with a finite speed,  $d\phi_i/dt \neq 0$ . Next, we can evaluate the order parameter using the stationary probability density in Eq. (9) as

$$r e^{i\theta} = \frac{1}{N} \sum_i \int_{-\infty}^{\infty} d\omega g(\omega) \int d\phi \rho_i^{(s)}(\phi|\omega) e^{i\phi}. \quad (10)$$

Although  $\bar{r}_i$ ,  $\bar{\theta}_i$ , and  $\rho_i^{(s)}(\phi|\omega)$  can fluctuate over  $i$  in the steady state, we assume here that they depend only on degree  $k_i$ . This is a mean field approximation. Keeping only the degree-dependent fluctuations, one can obtain a self-consistent equation for the local field through

Eq. (7) as

$$\bar{r}(k)e^{i\bar{\theta}(k)} = \sum_{k'=1}^{k_m} P(k'|k) \times \int_{-\infty}^{\infty} d\omega g(\omega) \int_0^{2\pi} d\phi \rho^{(s)}(\phi|\omega, k') e^{i\phi}, \quad (11)$$

where  $\rho^{(s)}(\phi|\omega, k)$  is given by the right hand side of Eq. (9) with  $\omega_*(k) = J\bar{r}(k)k^\eta$  replacing  $\omega_{*,i}$ .  $P(k'|k)$  denotes the probability that a neighboring vertex of a given vertex with degree  $k$  has degree  $k'$ , and  $k_m$  is the natural cutoff of degree. Here, we consider only the case that the network is random and does not have any type of degree-degree correlation; then,  $P(k'|k)$  can be written as  $k'P_d(k')/\langle k \rangle$  with  $\langle k \rangle = \sum_k kP_d(k)$ . After that, one can see that both  $\bar{r}(k)$  and  $\bar{\theta}(k)$  are independent of degree  $k$ , and therefore, we can drop the  $k$ -dependence in  $\bar{r}$  and  $\bar{\theta}$  from now on.

The last integral of Eq. (11) is evaluated as

$$\int_0^{2\pi} d\phi \rho^{(s)}(\phi|\omega, k) e^{i\phi} = e^{i\bar{\theta}} \begin{cases} i(\omega/\omega_*(k)) - i\sqrt{(\omega/\omega_*(k))^2 - 1}, & (\omega > \omega_*(k)), \\ i(\omega/\omega_*(k)) + \sqrt{1 - (\omega/\omega_*(k))^2}, & (|\omega| \leq \omega_*(k)), \\ i(\omega/\omega_*(k)) + i\sqrt{(\omega/\omega_*(k))^2 - 1}, & (\omega < -\omega_*(k)). \end{cases} \quad (12)$$

The remaining integration in Eq.(11) for  $\omega > \omega_*(k)$  and  $\omega < -\omega_*(k)$  cancel out due to the fact  $g(\omega) = g(-\omega)$ . As a result, only the oscillators having the frequency within the range  $|\omega| \leq \omega_*(k)$  contribute to the local field in Eq. (7). Thus, one obtains

$$\bar{r} = \sum_{k=1}^{k_m} \frac{kP_d(k)}{\langle k \rangle} \int_{-\omega_*(k)}^{\omega_*(k)} d\omega g(\omega) \sqrt{1 - \left(\frac{\omega}{\omega_*(k)}\right)^2}, \quad (13)$$

which is the self-consistent equation for  $\bar{r}$ . Note that  $\bar{r}$  is contained in  $\omega_*(k) = J\bar{r}k^\eta$ . After the local field is obtained, the order parameter in Eqs. (4) or (10) is calculated as

$$r = \sum_{k=1}^{k_m} P_d(k) \int_{-\omega_*(k)}^{\omega_*(k)} d\omega g(\omega) \sqrt{1 - \left(\frac{\omega}{\omega_*(k)}\right)^2}. \quad (14)$$

### III. SYNCHRONIZATION TRANSITION

In this section, we solve the self-consistent equation, Eq. (13) explicitly, and then investigate the behavior of the order parameter near the critical point via Eq. (14). To proceed, we first recall that the degree distribution is given in a closed form as  $P_d(k) = k^{-\lambda}/H_{k_m}^\lambda$  for  $\lambda > 2$ , where  $H_{k_m}^\lambda$  is the generalized harmonic number, defined by  $H_m^q \equiv \sum_{k=1}^m k^{-q}$  and  $k_m \sim N^{1/(\lambda-1)}$ . Substituting

$g(\omega) = e^{-\omega^2/2}/\sqrt{2\pi}$  to Eq. (13), one can derive the local field  $\bar{r}$  as

$$\begin{aligned} \bar{r} &= \sum_{k=1}^{k_m} \frac{kP_d(k)}{\langle k \rangle} \omega_*(k) \int_{-\pi/2}^{\pi/2} d\phi \cos^2 \phi \frac{1}{\sqrt{2\pi}} e^{-[\omega_*(k) \sin \phi]^2/2} \\ &= \sum_{n=0}^{\infty} \frac{(n-1/2)! (-1)^n H_{k_m}^{\lambda-\eta-2n\eta-1}}{n! (n+1)! 2^{n+3/2} H_{k_m}^{\lambda-1}} (J\bar{r})^{2n+1} \\ &\equiv \sum_{n=0}^{\infty} \bar{A}_n (J\bar{r})^{2n+1}, \end{aligned} \quad (15)$$

where we used the Taylor expansion of  $e^{-(\omega_*(k) \sin \phi)^2/2}$  and the integration  $\int_{-\pi/2}^{\pi/2} d\phi \cos^2 \phi \sin^{2n} \phi = \pi^{1/2} (n-1/2)! / (2(n+1)!)$ . Similarly, the order parameter is evaluated as

$$\begin{aligned} r &= \sum_{n=0}^{\infty} \frac{(n-1/2)! (-1)^n H_{k_m}^{\lambda-\eta-2n\eta}}{2^{n+3/2} n! (n+1)! H_{k_m}^\lambda} (J\bar{r})^{2n+1} \\ &\equiv \sum_{n=0}^{\infty} A_n (J\bar{r})^{2n+1}. \end{aligned} \quad (16)$$

If  $\eta \leq 0$ , the generalized harmonic numbers in  $\bar{A}_n$  and  $A_n$  are finite, and then they can be represented in terms of the Riemann zeta functions for all  $n$  below and they are denoted as  $\bar{B}_n$  and  $B_n$ , respectively. That is,

$$\bar{A}_n \approx \bar{B}_n = \frac{(n-1/2)! (-1)^n \zeta(\lambda - \eta - 2n\eta - 1)}{2^{n+3/2} n! (n+1)! \zeta(\lambda - 1)} \quad (17)$$

and

$$A_n \approx B_n = \frac{(n-1/2)! (-1)^n \zeta(\lambda - \eta - 2n\eta)}{2^{n+3/2} n! (n+1)! \zeta(\lambda)}, \quad (18)$$

respectively. Using these formulae, the local field and the order parameter are determined by Eqs. (15) and (16).

On the other hand, it is remarkable that when  $0 < q < 1$ , the generalized harmonic number diverges as  $H_m^q \simeq (m+1)^{1-q}/(1-q) + \zeta(q) + \mathcal{O}(m^{-q})$  in the  $m \rightarrow \infty$  limit, which is shown in Appendix. Then, Eqs. (15) and (16) are divided into analytic and singular parts as

$$\bar{r} = \sum_n \bar{B}_n (J\bar{r})^{2n+1} + \bar{C} (J\bar{r} k_m^\eta) (J\bar{r})^{(\lambda-2)/\eta} \quad (19)$$

and

$$r = \sum_n B_n (J\bar{r})^{2n+1} + C (J\bar{r} k_m^\eta) (J\bar{r})^{(\lambda-1)/\eta}, \quad (20)$$

respectively, where the functions  $\bar{C}(x)$  and  $C(x)$  are defined in Appendix. In the  $x \rightarrow \infty$  limit corresponding to the thermodynamic limit,  $\bar{C}(x)$  and  $C(x)$  reduce to  $\bar{C}_\infty$  and  $C_\infty$ , respectively, defined as

$$\begin{aligned} \bar{C}_\infty &= \frac{[(\lambda - 2\eta - 2)/2\eta]! [(2 - \lambda - \eta)/2\eta]!}{\eta 2^{(\lambda+4\eta-2)/2\eta} [(\lambda + \eta - 2)/2\eta]! \zeta(\lambda - 1)}, \\ C_\infty &= \frac{[(\lambda - 2\eta - 1)/2\eta]! [(1 - \lambda - \eta)/2\eta]!}{\eta 2^{(\lambda+4\eta-1)/2\eta} [(\lambda + \eta - 1)/2\eta]! \zeta(\lambda)}. \end{aligned} \quad (21)$$

Thus, the local field and the order parameter are written as

$$\bar{r} = \sum_{n=0}^{\infty} \bar{B}_n (J\bar{r})^{2n+1} + \bar{C}_{\infty} (J\bar{r})^{(\lambda-2)/\eta} + \dots, \quad (22)$$

and

$$r = \sum_{n=0}^{\infty} B_n (J\bar{r})^{2n+1} + C_{\infty} (J\bar{r})^{(\lambda-1)/\eta} + \dots, \quad (23)$$

for  $J\bar{r}k_m^{\eta} \gg 1$ . We remark that the singular terms appear only in the limit  $J\bar{r}k_m^{\eta} \rightarrow \infty$ . For the case of  $J\bar{r}k_m^{\eta} \ll 1$ , however, Eqs. (15) and (16) are valid.

Next, we determine the critical point. To proceed, we investigate the behavior of the local field as a function of  $J$ , which depends on the sign of  $\eta$ .

**(i) In the case of  $\eta \leq 0$ ,**  $\bar{A}_n$  and  $A_n$  are finite. One can see from Eq. (15) that the local field is zero for  $\bar{A}_0 J < 1$  and non-zero for  $\bar{A}_0 J > 1$ . The order parameter behaves in the same manner as that of the local field from Eq. (16). Thus, we obtain the critical point as

$$J_c = \frac{1}{\bar{A}_0} = \frac{2\sqrt{2}}{\sqrt{\pi}} \frac{H_{k_m}^{\lambda-1}}{H_{k_m}^{\lambda-1-\eta}}. \quad (24)$$

As  $\lambda \rightarrow \infty$ , the critical point  $J_c$  approaches  $2\sqrt{2}/\sqrt{\pi} \simeq 1.60$  in the limit  $N \rightarrow \infty$ , which is consistent with that found in case of the globally-coupled oscillators [7].

When  $J > J_c$ , the local field  $\bar{r}$  and the order parameter  $r$  are non-zero. When  $J$  is close to  $J_c$ ,

$$\bar{r} \simeq (|\bar{A}_1|J_c^3)^{-1/2} \Delta^{1/2} \quad (25)$$

and

$$r \simeq A_0 (|\bar{A}_1|J_c)^{-1/2} \Delta^{1/2}, \quad (26)$$

where  $\Delta = (J - J_c)/J_c$ . Thus, we obtain that  $\beta = 1/2$ . Again, this result is consistent with the one obtained from the globally-coupled oscillators [7].

**(ii) In the case of  $\eta > 0$ ,** the singular terms in Eqs. (22) and (23) can be crucial in determining the critical point and the order parameter. Depending on relative magnitude of  $\lambda$  and  $\eta$ , we divide the case of  $\eta > 0$  into four subcases:

- (I) When  $0 < \eta < (\lambda - 2)/3$  (i.e.,  $\lambda > 3\eta + 2$ ),  $\bar{r} \simeq \bar{B}_0 J\bar{r} + \bar{B}_1 J^3 \bar{r}^3 + \dots$  for small  $\bar{r}$  from Eq. (22). Then  $J_c$  and  $\bar{r}$  behave as those for  $\eta < 0$  presented in Eqs. (24) and (25).
- (II) When  $(\lambda - 2)/3 < \eta < \lambda - 2$  (i.e.,  $\eta + 2 < \lambda < 3\eta + 2$ ), the dominant contribution is made from the singular term of Eq. (22). Then

$$\bar{r} \simeq \bar{B}_0 J\bar{r} + \bar{C}_{\infty} (J\bar{r})^{(\lambda-2)/\eta} + \dots, \quad (27)$$

leading to

$$J_c \sim 1/\bar{B}_0 = \frac{2\sqrt{2}}{\sqrt{\pi}} \frac{\zeta(\lambda-1)}{\zeta(\lambda-\eta-1)} \quad (28)$$

and

$$\bar{r} \sim r \sim \Delta^{\eta/(\lambda-2-\eta)}. \quad (29)$$

- (III) When  $\lambda - 2 < \eta < \lambda - 1$  (i.e.,  $\eta + 1 < \lambda < \eta + 2$ ), the critical point in Eq. (24) for finite  $N$  behaves as

$$J_c \sim k_m^{-(\eta-\lambda+2)} \sim N^{-(\eta-\lambda+2)/(\lambda-1)}. \quad (30)$$

Thus, it approaches zero in the thermodynamic limit.  $\bar{r}$  is always positive unless  $J$  is zero as  $\bar{r} \sim J^{(\lambda-2)/(\eta-\lambda+2)}$  for small  $J$  and  $r \sim J\bar{r} \sim J^{\eta/(\eta-\lambda+2)}$ .

- (IV) When  $\eta > \lambda - 1$  (i.e.,  $\lambda < \eta + 1$ ), we obtain that  $r \sim (J\bar{r})^{(\lambda-1)/\eta}$ . Using the result of  $\bar{r}$  obtained in (III), we obtain that

$$r \sim J^{(\lambda-1)/(\eta-\lambda+2)}. \quad (31)$$

We summarize the result as follows: When  $\eta < \lambda - 2$  (in the (I) and (II) cases), the critical point  $J_c$  is finite; however, when  $\eta > \lambda - 2$  (in the (III) and (IV) cases),  $J_c = 0$  in the thermodynamic limit  $N \rightarrow \infty$ . Thus, the critical exponent  $\beta$  associated with the order parameter is defined through the relation,  $r \sim \Delta^{\beta}$  ( $r \sim J^{\beta}$ ) for the former (latter) case. The exponent  $\beta$  is evaluated in each case as follows:

$$\beta = \begin{cases} 1/2 & \text{in (I),} \\ \eta/(\lambda - 2 - \eta) & \text{in (II),} \\ \eta/(\eta - \lambda + 2) & \text{in (III),} \\ (\lambda - 1)/(\eta - \lambda + 2) & \text{in (IV).} \end{cases} \quad (32)$$

The result of the critical point is consistent with those of other phase transition problems such as the percolation transition and the epidemic spreading in SF networks. Moreover, the result for the case of  $\eta = 1$  reduces to the previous result [8, 9]. Moreover, the result  $\beta = 1/2$  for  $\eta = 1$  and  $\lambda > 5$  is reduced to the mean-field result in regular lattice.

#### IV. CLUSTER FORMATION OF SYNCHRONIZED OSCILLATORS

In this section, we investigate in detail how the coupled oscillator system develops its synchrony as the coupling strength increases. To this end, we study the formation of clusters comprising synchronized vertices as a function of the coupling strength  $J$ . We use the generating function approach to derive the cluster-size distribution.

### A. Cooperative versus background synchrony

The order parameter averaged over the natural frequency distribution  $g(\omega)$  can be written as

$$r = \frac{1}{N} \sqrt{\sum_i \langle \cos^2 \phi_i + \sin^2 \phi_i \rangle + \sum_i \sum_{j \neq i} \langle \cos(\phi_i - \phi_j) \rangle} \quad (33)$$

from Eq.(4). Here, the brackets represent the average over  $g(\omega)$ . For the case of  $J = 0$ , each element oscillates independently, so that  $\langle \cos(\phi_i - \phi_j) \rangle = 0$  for  $i \neq j$ . Thus, the order parameter is evaluated as

$$r_{J=0} \sim \frac{1}{\sqrt{N}}. \quad (34)$$

As  $J$  increases, clusters comprising synchronized oscillators are more likely to form. We here define a cluster as a group of vertices (or oscillators) which are connected and in the same coherent state: Two oscillators are coherent if its time-average correlation function  $C_{ij}$ , defined as

$$C_{ij} = \frac{1}{(t_1 - t_0)} \sum_{t=t_0+1}^{t_1} \langle \cos(\phi_i(t) - \phi_j(t)) \rangle, \quad (35)$$

is larger than a preassigned threshold value  $C_{th}$ . We choose  $C_{th}$  value to generate the cluster-size distribution in a power law form at the critical point  $J_c$ . As such clusters form, the term of  $\sum_i \sum_{j \neq i} \langle \cos(\phi_i - \phi_j) \rangle$  becomes nonzero and dominant. The order parameter is then evaluated as

$$r \sim \frac{\sqrt{\sum_{\kappa} s_{\kappa}^2}}{N}, \quad (36)$$

where  $\kappa$  is the index of cluster and  $s_{\kappa}$  is the size of cluster  $\kappa$ , i.e., the number of vertices within the cluster  $\kappa$ . Note that  $\sum_{\kappa} s_{\kappa} = N$ , and Eq. (36) reduces to Eq. (34) when  $J = 0$  because each cluster size is 1. In the synchronized state when  $J \gg J_c$ , the size of the largest cluster, denoted as  $S$ , is of  $\mathcal{O}(N)$ , and thus the order parameter is approximately given as

$$r \sim S/N. \quad (37)$$

Next, we study the cluster-size distribution and the size of the largest cluster as a function of  $J$ .

The dynamics of cluster merging with increasing  $J$  results in the change of the cluster-size distribution. Let  $n(s)$  be the number of  $s$ -size clusters. Then  $\sum_s sn(s) = N$ . The cluster-size distribution is defined as  $n(s)/\sum_s n(s)$ . For  $J < J_c$ , the cluster-size distribution decays exponentially for large  $s$ . However, it decays in the power law form (3) at the critical point  $J = J_c$ , and the associated exponent  $\tau$  depends on the parameters  $\eta$  and  $\lambda$ . We determine  $\tau$  using the generating function method in the next subsection. For  $J > J_c$ , a giant cluster forms and the distribution of finite-size clusters decays exponentially. The cluster-size distributions for various values of  $J$  are shown in Fig. 1.

### B. Generating function of the cluster-size distribution

The probability that a vertex belongs to a cluster with size  $s$  is given by  $sn(s)/N$ , which is denoted as  $p(s)$ . Invoking the percolation theory,  $p(s)$  follows a power law with an exponential cutoff,

$$p(s) \sim s^{-\tau} e^{-s/s_c}, \quad (38)$$

where  $s_c$  is the characteristic size, which depends on  $J$  and system size  $N$ . In the thermodynamic limit  $N \rightarrow \infty$ ,  $s_c$  diverges at  $J = J_c$ . As in the percolation theory, the generating function  $\mathcal{P}(z) \equiv \sum_s p(s)z^s$  is useful for studying structural feature of the synchronized clusters, since its singular behavior is related to the critical behavior of the synchronization transition. (i) The order parameter  $r \sim S/N$  can be obtained from the relation  $r \simeq \lim_{N \rightarrow \infty} [1 - \mathcal{P}(z_N^*)]$ , where  $\mathcal{P}(z_N^*) = \sum_{s < S} p(s)$ , i.e., the contribution by finite-size clusters. This can be achieved by choosing  $z_N^* \approx e^{-1/S_m}$ , where  $S_m$  is a cluster size smaller than the largest cluster but larger than the second largest cluster. (ii) From Eq. (38), one can find that  $\mathcal{P}(z)$  diverges for  $z > z_c = \lim_{s \rightarrow \infty} p(s)^{-1/s}$ , i.e.,  $z_c \approx e^{1/s_c}$ . Thus, at  $J = J_c$ ,  $\mathcal{P}(z) \sim (1 - z)^{\tau-1}$  as  $z \rightarrow z_c = 1$  in the thermodynamic limit. Thus, finding the singularity of  $\mathcal{P}(z)$  enables one to obtain  $p(s)$ .

For the purpose, we introduce another generating function  $\bar{\mathcal{P}}(z)$  as a partner of the local field  $\bar{r}$ . From  $\bar{\mathcal{P}}(z)$ , one can define a probability  $\bar{p}(s)$  via the relation  $\bar{\mathcal{P}}(z) \equiv \sum_s \bar{p}(s)z^s$ , where  $\bar{p}(s)$  is defined similarly to  $p(s)$  as the probability that a vertex belongs to a synchronized cluster of size  $s$  composed of the vertex and  $s - 1$  neighboring vertices. For finite  $N$ , the generating function  $\bar{\mathcal{P}}(z)$  is analytic for  $|z| \leq 1$  and so is its inverse function  $\bar{\mathcal{P}}^{-1}(z)$ . To investigate the singularity of  $\bar{\mathcal{P}}(z)$  near  $z = 1$ , we consider the expansion of the inverse function  $z = \bar{\mathcal{P}}^{-1}(\omega) = 1 - \sum_{n \geq 1} b_n(1 - \omega)^n$  around  $\omega = 1$ . The coefficient  $b_n$  depends on  $J$ . Using Eqs. (15) and (22) and replacing  $\bar{r}$  by  $1 - \omega$ , we can find that the generating function  $\bar{\mathcal{P}}(z)$  satisfies the self-consistent relations given below:

$$z = \bar{\mathcal{P}}(z) + \sum_{n=0}^{\infty} \bar{B}_n [J(1 - \bar{\mathcal{P}}(z))]^{2n+1} + \bar{C}_{\infty} [J(1 - \bar{\mathcal{P}}(z))]^{(\lambda-2)/\eta} + \dots, \quad (39)$$

for  $J(1 - \bar{\mathcal{P}}(z))k_m^{\eta} \gg 1$ , and

$$z = \bar{\mathcal{P}}(z) + \sum_{n=0}^{\infty} \bar{A}_n [J(1 - \bar{\mathcal{P}}(z))]^{2n+1}, \quad (40)$$

for  $J(1 - \bar{\mathcal{P}}(z))k_m^{\eta} \ll 1$ . Similarly,  $\mathcal{P}(z)$  is determined as

$$z - \mathcal{P}(z) = \sum_{n=0}^{\infty} B_n [J(1 - \bar{\mathcal{P}}(z))]^{2n+1} + C_{\infty} [J(1 - \bar{\mathcal{P}}(z))]^{(\lambda-1)/\eta} + \dots, \quad (41)$$

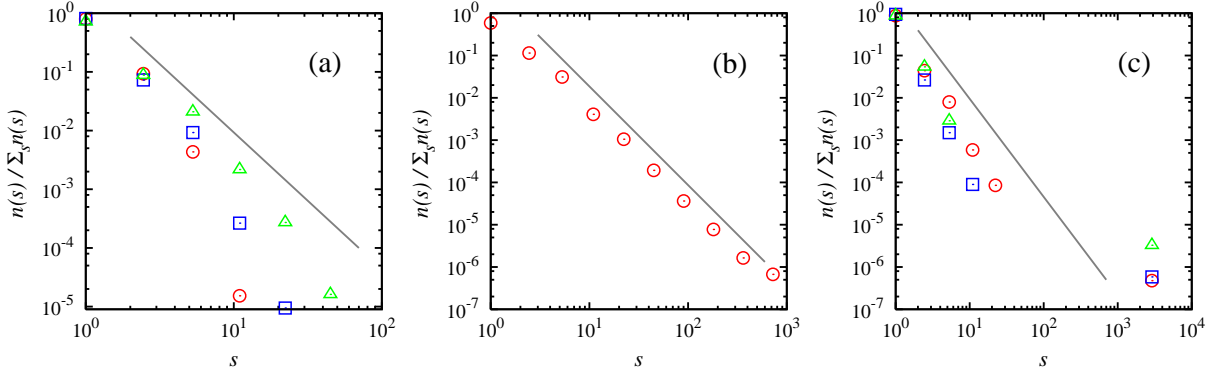


FIG. 1: (Color online) Cluster-size distributions  $n(s)/\sum_s n(s)$  of synchronized clusters for the networks generated with  $\lambda = 4.0$ ,  $\eta = 0.0$ , and  $N = 3000$  at  $J = 0.7J_c$  ( $\circ$ ),  $J = 0.8J_c$  ( $\square$ ),  $J = 0.9J_c$  ( $\triangle$ ) for (a),  $J = J_c$  ( $\circ$ ) for (b),  $J = 1.1J_c$  ( $\circ$ ),  $J = 1.2J_c$  ( $\square$ ), and  $J = 1.3J_c$  ( $\triangle$ ) for (c), respectively. Solid lines drawn for reference have a slope of  $7/3$  for all.

for  $J(1 - \bar{\mathcal{P}}(z))k_m^\eta \gg 1$ , and

$$z - \mathcal{P}(z) = \sum_{n=0}^{\infty} A_n [J(1 - \bar{\mathcal{P}}(z))]^{2n+1}, \quad (42)$$

for  $J(1 - \bar{\mathcal{P}}(z))k_m^\eta \ll 1$ .

### C. Behavior of $p(s)$ at the critical point

Here, we calculate the probability  $p(s)$  to find a vertex in the  $s$ -size cluster at the critical point  $J = J_c$  explicitly in each case defined in Sec.III.

**In the case (I)**, since  $\eta < (\lambda - 2)/3$ , we obtain that  $z = 1 + \bar{B}_1 (J_c(1 - \bar{\mathcal{P}}(z)))^3 + \dots$  to the leading orders by expanding  $z = \bar{\mathcal{P}}^{-1}(\omega)$  around  $\omega = 1$  in either Eqs. (39) or (40). Thus, we obtain that  $1 - \bar{\mathcal{P}}(z) \sim (1 - z)^{1/3}$ , leading to

$$\bar{p}(s) \sim s^{-4/3} \quad (43)$$

for large  $s$ .

Using the obtained leading behaviors of  $\bar{\mathcal{P}}(z)$  around  $z = 1$  in Eqs. (41) and (42), one obtains the behavior of  $\mathcal{P}(z)$  around  $z = 1$  as  $1 - \mathcal{P}(z) \sim (1 - z)^{1/3}$ . Thus,

$$p(s) \sim s^{-4/3}. \quad (44)$$

**In the case (II)**, the singular term in Eq. (39) is relevant. In this case, the behavior of  $\bar{\mathcal{P}}(z)$  for  $z < z_c$  differs from that for  $z > z_c$ .  $z_c$  is determined by the criterion  $J(1 - \bar{\mathcal{P}}(z_c))k_m^\eta \sim 1$ . This case also happens for the cases (III) and (IV).

In this case, the singular term  $\bar{C}_\infty [J_c(1 - \bar{\mathcal{P}}(z))]^{(\lambda-2)/\eta}$  is dominant in Eq. (39); therefore, it follows that  $1 - \bar{\mathcal{P}}(z) \sim J_c^{-1}(1 - z)^{\eta/(\lambda-2)}$  at  $J = J_c$ , which is valid for  $z \gg z_c$ . From this result,  $\bar{p}(s)$  is obtained as

$$\bar{p}(s) \sim J_c^{-1} s^{-(\eta+\lambda-2)/(\lambda-2)}, \quad (45)$$

which is valid for  $s \ll s_c$ .

On the other hand, when  $J(1 - \bar{\mathcal{P}}(z))k_m^\eta \ll 1$  so that  $|\bar{A}_{n+1}/\bar{A}_n| [J(1 - \bar{\mathcal{P}}(z))]^2 \ll 1$ , one can obtain that  $1 - \bar{\mathcal{P}}(z) \sim J_c^{-1} |\bar{A}_1|^{-1/3} (1 - z)^{1/3}$  for  $z \ll z_c$ ; therefore,

$$\bar{p}(s) \sim J_c^{-1} k_m^{(\lambda-2)/3 - \eta} s^{-4/3} \quad (46)$$

for large  $s \gg s_c$ .  $s_c$  is evaluated as follows: Substituting the result of  $1 - \bar{\mathcal{P}}(z)$  in the criterion  $J_c(1 - \bar{\mathcal{P}}(z_c))k_m^\eta \sim 1$  and using  $(1 - z_c) \sim s_c^{-1}$ , one can obtain system-size dependence of the characteristic size  $s_c$  explicitly as

$$s_c \sim k_m^{\lambda-2} \sim N^{(\lambda-2)/(\lambda-1)}, \quad (47)$$

which diverges as  $N \rightarrow \infty$ .

Together with Eqs. (45) and (46), we obtain that

$$\bar{p}(s) \sim \begin{cases} s^{-(\eta+\lambda-2)/(\lambda-2)} & (s \ll s_c), \\ k_m^{(\lambda-2)/3 - \eta} s^{-4/3} & (s \gg s_c). \end{cases} \quad (48)$$

Next, using the result of  $1 - \mathcal{P}(z) \sim 1 - \bar{\mathcal{P}}(z)$  obtained from both Eqs. (41) and (42), one can find that  $p(s)$  behaves similarly to  $\bar{p}(s)$ . That is,

$$p(s) \sim \begin{cases} s^{-(\eta+\lambda-2)/(\lambda-2)} & (s \ll s_c), \\ k_m^{(\lambda-2)/3 - \eta} s^{-4/3} & (s \gg s_c). \end{cases} \quad (49)$$

**In the case (III)**, the critical point  $J_c$  is finite in finite-size systems as being of order  $J_c \sim k_m^{\lambda-2-\eta} \sim N^{(\lambda-2-\eta)/(\lambda-1)}$ . Plugging the  $N$ -dependence into Eq. (46) and the expression,  $1 - \bar{\mathcal{P}}(z) \simeq 1 - z + \bar{C}_\infty [J_c(1 - z)]^{(\lambda-2)/\eta}$  for  $s \ll s_c$  from Eq. (39), one obtains  $\bar{p}(s)$  as follows:

$$\bar{p}(s) \sim \begin{cases} k_m^{(\lambda-2-\eta)(\lambda-2)/\eta} s^{-(\lambda-2+\eta)/\eta} & (s \ll s_c), \\ k_m^{-2(\lambda-2)/3} s^{-4/3} & (s \gg s_c). \end{cases} \quad (50)$$

Next, we derive  $p(s)$ . We find that the leading singular term in  $\mathcal{P}(z)$  for the case  $1 - z \gg s_c^{-1} \sim k_m^{2-\lambda}$  shows up in two ways. Substituting  $1 - \bar{\mathcal{P}}(z) \approx 1 - z + \bar{C}_\infty [J_c(1 -$

$z)]^{(\lambda-2)/\eta}$  to Eq. (41), we obtain that  $1-\mathcal{P}(z) \approx B_0 J_c (1-z) + B_0 J_c \bar{C}_\infty [J_c (1-z)]^{(\lambda-2)/\eta} + C_\infty [J_c (1-z)]^{(\lambda-1)/\eta} + \dots$ . We compare the second with the third terms in order of magnitude. Using the fact that  $J_c \sim k_m^{\lambda-2-\eta}$ , we find that there exist two subcases for  $s \ll s_c$ . The second term  $B_0 J_c \bar{C}_\infty [J_c (1-z)]^{(\lambda-2)/\eta}$  is more dominant than the third term  $C_\infty [J_c (1-z)]^{(\lambda-1)/\eta}$  when  $1-z \ll s_*^{-1}$  and vice versa. Here, it is found that a new crossover size  $s_*$  scales as

$$s_* \sim k_m^{(\eta-1)(\eta-\lambda+2)}. \quad (51)$$

From the behaviors of  $\mathcal{P}(z)$  in the three different subcases, we obtain the probability  $p(s)$  as

$$p(s) \sim \begin{cases} k_m^{(\lambda-1)(\lambda-2-\eta)/\eta} s^{-(\lambda-1+\eta)/\eta} & (s \ll s_*), \\ k_m^{(\lambda-2-\eta)(\lambda-2+\eta)/\eta} s^{-(\lambda-2+\eta)/\eta} & (s_* \ll s \ll s_c), \\ k_m^{(\lambda-2)/3-\eta} s^{-4/3} & (s \gg s_c). \end{cases} \quad (52)$$

One can notice that the subcase  $s \ll s_*$  diminishes when  $\eta \leq 1$ , but it is extended as the parameter  $\eta$  increases.

**In the case (IV)**, the third term  $C_\infty [J_c (1-z)]^{(\lambda-1)/\eta}$  in  $1-\mathcal{P}(z)$  in the case (III) is always dominant when  $1-z \gg s_c^{-1}$ . Moreover,  $A_0$  in Eq. (42) diverges as  $A_0 \sim k_m^{\eta-\lambda+1}$ , which has to be considered in the relation,  $1-\bar{P}(z) \simeq A_i J_c (1-\bar{P}(z))$  for  $1-z \ll s_c^{-1}$ . Consequently,  $p(s)$  behaves as

$$p(s) \sim \begin{cases} k_m^{(\lambda-1)(\lambda-2-\eta)/\eta} s^{-(\lambda-1+\eta)/\eta} & (s \ll s_c), \\ k_m^{(1-2\lambda)/3} s^{-4/3} & (s \gg s_c). \end{cases} \quad (53)$$

To substantiate the predictions of this section, we investigate the asymptotic behavior of  $p(s)$  in a numerical manner. The static model introduced in [11] is used for underlying network in our simulations. The network has  $N = 3000$  oscillators and its mean degree  $\langle k \rangle$  is 4.0. The values of  $\lambda$  and  $\eta$  are chosen as 4.0 and 0.0, respectively. This pair belongs to the case (I). First, we simulate the system at  $J = J_c$  to determine  $C_{\text{th}}$  defined in Sec. IV A. During the simulation, we assume a large value of  $C_{\text{th}}$  and then collect the pairs of vertices that the  $C_{ij}$  of each pair is larger than the assumed  $C_{\text{th}}$ . After that, we determine clusters and obtain the cluster-size distribution. We then adjust  $C_{\text{th}}$  by somewhat decreasing or increasing it, and repeat these procedures until the power-law distribution appears in the cluster-size distribution. If the cluster-size distribution follows the power-law form of  $p(s) \sim s^{-\tau}$ , the corresponding value of  $C_{\text{th}}$  is considered as the threshold value  $C_{\text{th}}$ . It is found numerically that  $C_{\text{th}} \approx 0.7$ , independent of the system size  $N$ . In our simulations, we obtain  $\tau + 1 \approx 7/3$ , which is close to the theoretical value in Eq. (44), as shown in Fig. 1(b). We also performed simulations for various  $J < J_c$  and  $> J_c$  as shown in Figs. 1(a) and (c), respectively. The power-law behaviors in the cluster-size distribution do not appear in these cases.

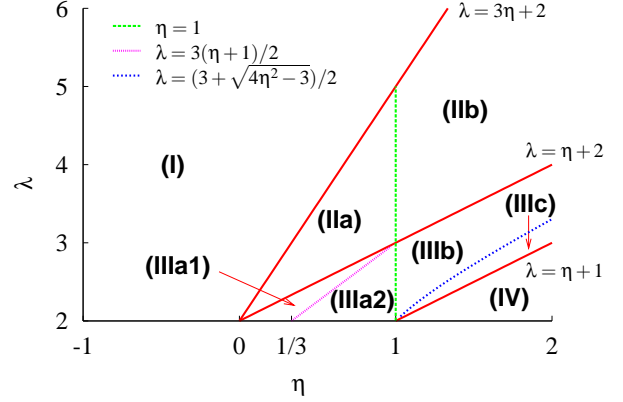


FIG. 2: (Color online) Diagram in the space of  $(\eta, \lambda)$  of eight different domains each corresponding to a distinct synchronization transition. The transition nature of each domain is listed in Table I.

## V. LARGEST CLUSTER SIZE AND FINITE-SIZE SCALING

In this section, we first investigate the  $N$ -dependence of the largest cluster size at  $J_c$ . Next, based on this result, we derive a finite-size scaling form for the order parameter near  $J_c$ .

### A. The largest cluster size

The largest cluster size  $S$  can be obtained from the relation [13],

$$\sum_{s>S} p(s) \sim \frac{S}{N}. \quad (54)$$

**In the case (I)**, we use the result of Eq. (44), and obtain simply that

$$S \sim N^{3/4}. \quad (55)$$

**In the case (II)**,  $p(s)$  displays a crossover at  $s_c$ , and thus the obtained value of the largest cluster size must satisfy the self-consistency conditions. For instance, the largest cluster size obtained by Eq. (54) for  $s \ll s_c$  in Eq. (49) has to be smaller than  $s_c$ . As a result, the largest cluster size behaves differently in the two subcases  $\eta < 1$  and  $\eta \geq 1$ , which we denote (IIa) and (IIb), respectively. In each subcase, we obtain that

$$S \sim \begin{cases} N^{(4\lambda-5-3\eta)/[4(\lambda-1)]} & \text{in (IIa),} \\ N^{(\lambda-2)/(\lambda-2+\eta)} & \text{in (IIb).} \end{cases} \quad (56)$$

The largest cluster size  $S$  in (IIa) was determined from  $p(s)$  for  $s \gg s_c$ , and is indeed much larger than  $s_c$ , whereas it in (IIb) was done from  $p(s)$  for  $s \ll s_c$ .

TABLE I: The probability to find a vertex in  $s$ -size cluster  $p(s)$ , the largest cluster size  $S$  at the critical point, and the critical exponents  $\beta$  and  $\mu$  for the eight cases shown in Fig. 2.

domain	$p(s)$	$S$	$\beta$	$\mu$
(I)	$s^{-4/3}$	$N^{3/4}$	$\frac{1}{2}$	2
(IIa)	$\begin{cases} s^{-(\eta+\lambda-2)/(\lambda-2)} & (s \ll s_c), \\ k_m^{(\lambda-2)/3-\eta} s^{-4/3} & (s \gg s_c) \end{cases}$	$N^{(4\lambda-5-3\eta)/[4(\lambda-1)]}$	$\frac{\eta}{\lambda-2-\eta}$	$\frac{\eta}{1+3\eta} \frac{4(\lambda-1)}{\lambda-2-\eta}$
(IIb)		$N^{(\lambda-2)/(\lambda-2+\eta)}$		$\frac{\lambda-2+\eta}{\lambda-2-\eta}$
(IIIa1)	$\begin{cases} k_m^{(\lambda-1)(\lambda-2-\eta)/\eta} s^{-(\lambda-1+\eta)/\eta} & (s \ll s_*) \\ k_m^{(\lambda-2-\eta)(\lambda-2+\eta)/\eta} s^{-(\lambda-2+\eta)/\eta} & (s_* \ll s \ll s_c) \\ k_m^{(\lambda-2)/3-\eta} s^{-4/3} & (s \gg s_c). \end{cases}$	$N^{(4\lambda-5-3\eta)/[4(\lambda-1)]}$	$\frac{\eta}{\eta-\lambda+2}$	$\frac{\eta}{1+3\eta} \frac{4(\lambda-1)}{\eta-\lambda+2}$
(IIIa2)		$N^{\eta/(\lambda-2+\eta)+(\lambda-2-\eta)/(\lambda-1)}$		$\frac{2\eta}{\eta-\lambda+2}$
(IIIb)		$N^{(\lambda-2)/(\lambda-1+\eta)}$		
(IIIc)				
(IV)	$\begin{cases} k_m^{(\lambda-1)(\lambda-2-\eta)/\eta} s^{-(\lambda-1+\eta)/\eta} & (s \ll s_c) \\ k_m^{(1-2\lambda)/3} s^{-4/3} & (s \gg s_c). \end{cases}$	$N^{(\lambda-2)/(\lambda-1+\eta)}$	$\frac{\lambda-1}{\eta-\lambda+2}$	$\frac{2(\lambda-1)}{\eta-\lambda+2}$

In the case (III),  $p(s)$  exhibits three distinct power-law behaviors. Thus, this case is divided into three subcases. They are as follows:  $\eta < 1$  (IIIa),  $1 \leq \eta \leq \sqrt{\lambda^2 - 3\lambda + 3}$  (IIIb), and  $\eta > \sqrt{\lambda^2 - 3\lambda + 3}$  (IIIc). The largest cluster size in each subcase is given as

$$S \sim \begin{cases} N^{(4\lambda-5-3\eta)/[4(\lambda-1)]} & \text{in (IIIa),} \\ N^{\eta/(\lambda-2+\eta)+(\lambda-2-\eta)/(\lambda-1)} & \text{in (IIIb),} \\ N^{(\lambda-2)/(\lambda-1+\eta)} & \text{in (IIIc).} \end{cases} \quad (57)$$

In the case (IV), the largest cluster size is determined simply by  $p(s)$  for  $s \ll s_c$  since the resulting largest cluster size fulfils the criterion  $S < s_c$  for  $\eta > 0$ . Thus,

$$S \sim N^{(\lambda-2)/(\lambda-1+\eta)}. \quad (58)$$

## B. Finite-size scaling

Here, we evaluate the magnitude of the order parameter  $r_c$  at  $J_c$  and establish the finite-size scaling function. To proceed, we compare the magnitude of cooperative synchrony  $S/N$  with that of the background synchrony  $\sim N^{-1/2}$ . The order parameter  $r_c$  is defined as  $\sim S/N$  if  $S/N \gg N^{-1/2}$ , and  $\sim N^{-1/2}$  otherwise. Under this criterion, we obtain  $r_c$  as  $\sim S/N$  in the cases (I) and (II), and  $\sim N^{-1/2}$  in the cases (IIIb), (IIIc), and (IV). The case (IIIa) is divided into two subcases,  $2\lambda - 3\eta - 3 \geq (<) 0$ . They are denoted as (IIIa1) and (IIIa2), respectively. The order parameter  $r_c$  behaves as  $\sim S/N$  and  $\sim N^{-1/2}$  in (IIIa1) and (IIIa2), respectively.

By using that  $r \sim \Delta^\beta$  and  $N$ -dependent behavior of  $r_c$  at  $J_c$ , we can construct a finite-size scaling form as

$$r = N^{-\beta/\mu} \psi(\Delta N^{1/\mu}) \quad (59)$$

for the cases (I) and (II), and

$$r = N^{-\beta/\mu} \psi(JN^{1/\mu}) \quad (60)$$

for the cases (III) and (IV), where

$$\psi(x) \sim \begin{cases} \text{const} & \text{for } x \ll 1, \\ x^\beta & \text{for } x \gg 1. \end{cases} \quad (61)$$

The critical exponent  $\mu$  is determined by the relation  $r_c \sim N^{-\beta/\mu}$ . The value of  $\mu$  varies depending on the cases determined by the magnitude of  $\eta$  and  $\lambda$ .

We present the diagram in Fig. 2 comprising eight distinct cases in the  $(\eta, \lambda)$  plane. Each case in the diagram corresponds to a distinct behavior of the critical exponents  $\beta$  and  $\mu$ , the cluster-size distribution, and the largest cluster size. We summarize those features in Table I.

## VI. NUMERICAL SIMULATIONS

We perform direct numerical integration of Eq. (2) to confirm the analytic results. In particular, the finite-size scaling behaviors in Eqs. (59) and (60) are compared. For the purpose, we generate random SF networks using the static model [11] with system sizes of  $N = 400, 800, 1600$ , and 3200, mean degree of  $\langle k \rangle = 4.0$  and values of  $\eta$  and  $\lambda$  chosen from each domain in Fig. 2. Numerical values of  $(\lambda, \eta)$  we used are listed in Table II. For the numerical integration, we apply the Heun's method [12]. Time is discretized by a unit step  $\delta t = 0.005$  and runs up to  $t = 1.2 \times 10^4$ . Ensemble average is taken over  $\mathcal{O}(10^2) \sim \mathcal{O}(10^3)$  different configurations of natural frequencies and network realizations, respectively.

Numerical results are presented in Fig. 3. For each Fig. 3(a)–(c), the critical point  $J_c$  is finite. We find  $J_c$



TABLE II: Numerical values of the parameters  $(\eta, \lambda)$  we used for Figs. 3.  $\beta_t$  and  $\mu_t$  are theoretical values for a given set of  $(\eta, \lambda)$  in the third column.  $\beta_n$  and  $\mu_n$  are numerical values to draw Figs 3 for each case. For (a)–(c), the theoretical and numerical values are the same each other for both  $\beta$  and  $\mu$ . However, they can be different for (d)–(h).  $r_t$  and  $r_n$  are the order parameters in scaling form formulated with the theoretical values of  $\beta_t$  and  $\mu_t$ , and the numerical values  $\beta_n$  and  $\mu_n$ , respectively.

Fig. 3	domain	$(\eta, \lambda)$	$\beta_t$	$\beta_n$	$\mu_t$	$\mu_n$	$r_t$	$r_n$
(a)	(I)	(1/3, 4)	1/2	1/2	2	2	$N^{-1/4}\psi(\Delta N^{1/2})$	$N^{-1/4}\psi(\Delta N^{1/2})$
(b)	(IIa)	(5/6, 4)	5/7	5/7	49/120	49/120	$N^{-7/24}\psi(\Delta N^{49/120})$	$N^{-7/24}\psi(\Delta N^{49/120})$
(c)	(IIb)	(4/3, 4)	2	2	5	5	$N^{-2/5}\psi(\Delta N^{1/5})$	$N^{-2/5}\psi(\Delta N^{1/5})$
(d)	(IIIa1)	(1/3, 13/6)	2	20/7	14/3	20/3	$N^{-3/7}\psi(JN^{3/14})$	$N^{-3/7}\psi(JN^{3/20})$
(e)	(IIIa2)	(2/3, 13/6)	4/3	50/23	8/3	100/23	$N^{-1/2}\psi(JN^{3/8})$	$N^{-1/2}\psi(JN^{23/100})$
(f)	(IIIb)	(5/2, 4)	5	5	10	10	$N^{-1/2}\psi(JN^{1/10})$	$N^{-1/2}\psi(JN^{1/10})$
(g)	(IIIc)	(11/4, 4)	11/3	11/3	22/3	22/3	$N^{-1/2}\psi(JN^{3/22})$	$N^{-1/2}\psi(JN^{3/22})$
(h)	(IV)	(4, 4)	3/2	5	3	10	$N^{-1/2}\psi(JN^{1/3})$	$N^{-1/2}\psi(JN^{1/10})$

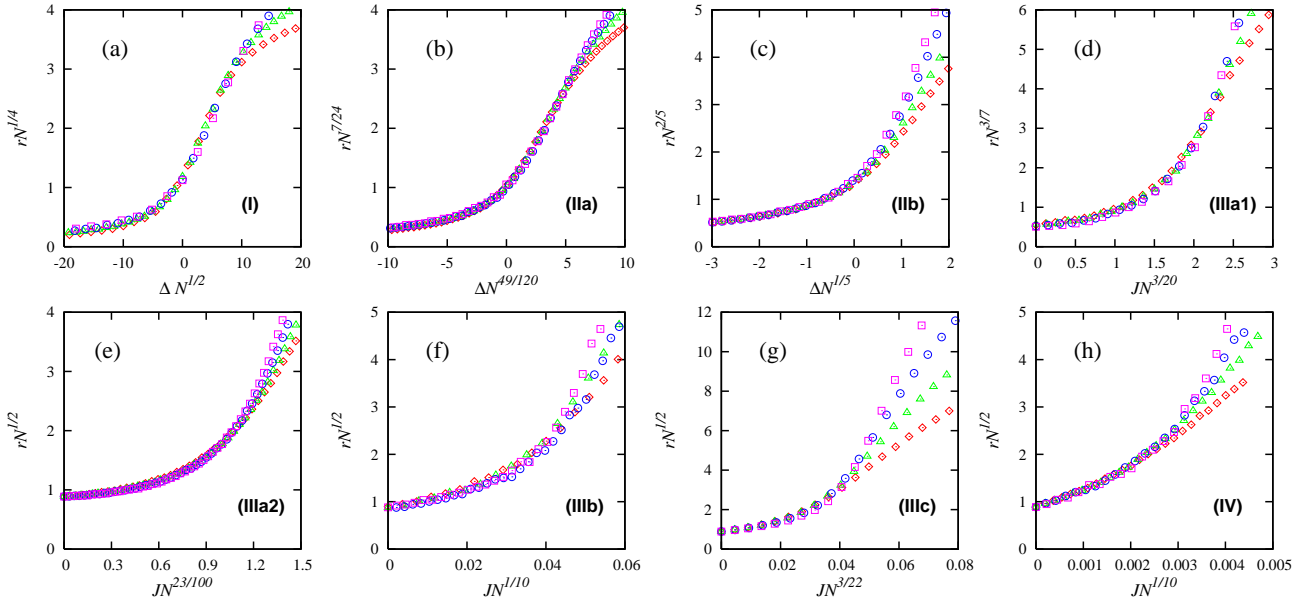


FIG. 3: (Color online) Finite-size scaling behaviors of the order parameter  $r$ . Data are collected from the static network model with mean degree  $\langle k \rangle = 4$  and system sizes  $N = 400$  ( $\diamond$ ),  $800$  ( $\triangle$ ),  $1600$  ( $\circ$ ), and  $3200$  ( $\square$ ). Numerical values of the tunable parameters  $(\eta, \lambda)$  and the critical exponents are given in Table. II for each case. For the critical point  $J_c$ , theoretical  $J_c^{(t)}$  and numerical  $J_c^{(n)}$  values used in (a)–(c) are different as  $(J_c^{(t)}, J_c^{(n)}) = (0.92, 1.32)$  (a),  $(0.37, 0.50)$  (b), and  $(0.13, 0.18)$  (c).

numerically to make the obtained numerical data collapsed for different system size  $N$  in the scaling plot with theoretical values of  $\beta$  and  $\mu$ . Theoretical and numerically found values of  $J_c$ , denoted as  $J_c^{(t)}$  and  $J_c^{(n)}$ , respectively, are compared as  $(J_c^{(t)}, J_c^{(n)}) = (0.92, 1.32)$  for (a),  $(0.37, 0.50)$  for (b), and  $(0.13, 0.18)$  for (c). They belong to the cases (I), (IIa), and (IIb), respectively.

For Figs.3 (d)–(h), the critical point  $J_c$  is zero. For the cases of (d), (e), and (h), we find that numerical data

do not collapse well in the scaling plot of  $rN^{\beta/\mu}$  versus  $JN^{1/\mu}$  with theoretical values of  $\beta_t$  and  $\mu_t$  tabulated in Table I. Instead, we adjust numerical values of  $\beta_n$  and  $\mu_n$  values empirically to make the obtained numerical data collapsed. Those empirical values of  $\beta_n$  and  $\mu_n$  are compared with the theoretical values as listed in Table II. The discrepancy in (d) and (e) originates from the presence of intrinsic degree-degree correlation in the static model when the degree exponent  $2 < \lambda < 3$ , while the

theoretical values were obtained under the assumption that the degree-degree correlation is absent.

## VII. CONCLUSIONS AND DISCUSSION

In this paper, we have investigated the nature of the synchronization transition generated by  $N$  limit-cycle oscillators located at random SF networks with degree exponent  $\lambda$ . The dynamics is given by a modified Kuramoto equation with the asymmetric and degree-dependent weighted coupling strength in the form of  $Jk_i^{1-\eta}$ , where  $k_i$  is the degree of vertex  $i$ . Depending on the sign and magnitude of  $\eta$ , the influence of the hub vertices on the dynamics can be moderated or amplified, and determines the nature of the synchronization transition. Applying the mean-field approach to the modified Kuramoto equation, we derived the critical point, the size distribution of synchronized clusters, and the largest cluster size at the critical point. The critical exponents associated with the order parameter and the finite-size scaling are determined in terms of the two tunable parameters,  $(\eta, \lambda)$ . All results are summarized in Table. I. The parameter space of  $(\eta, \lambda)$  is divided into eight different domains, in each of which the transition nature is distinct.

It would be interesting to notice that the critical exponents  $\beta$  and  $\mu$  associated with the order parameter and the finite-size scaling of the synchronization transition depend on the parameter  $\eta$  defined in the coupling strength. The result is unusual from the perspective of the universality in the critical phenomena in regular lattice where the details of the couplings are mostly irrelevant unless they are long ranged [15]. This result implies that structural features of SF networks such as the degree distribution are not sufficient to understand the dynamic process on such networks. Asymmetric coupling in dynamics is a relevant perturbation in such networks, because of the heterogeneity of the degree distribution. Such a behavior was also observed in the sandpile model [16].

## VIII. ACKNOWLEDGEMENT

This work was supported by KRF Grant No. R14-2002-059-010000-0 of the ABRL program funded by the Korean government (MOEHRD) and the Seoul R & BD program.

## APPENDIX A: DERIVATION OF EQS. (19-20)

In this Appendix, we present the derivation of Eqs. (19-20) from Eqs. (15) and (16) with  $\eta > 0$ . Since the right-hand-side of Eq. (16) becomes the same as that of Eq. (15) when  $\lambda$  is shifted by 1, we here analyze in

detail the nature of Eq. (15) only, which applies also to Eq. (16) with  $\lambda$  replaced by  $\lambda + 1$ .

The coefficients in Eq. (15) diverge with increasing  $N$  for  $n \geq n_c \equiv \lceil (\lambda - \eta - 2)/(2\eta) \rceil$ , where  $\lceil x \rceil$  is the smallest integer not smaller than  $x$ , due to the divergence of the generalized harmonic number  $H_m^q$  for  $0 < q < 1$ . While  $H_m^q \simeq \zeta(q)$  for  $q > 1$ ,  $H_m^q$  diverges in the limit  $m \rightarrow \infty$  for  $0 < q < 1$  and its asymptotic expansion can be obtained by using the relation  $H_m^q = \zeta(q) - \zeta(q, m+1)$  and the asymptotic expansion of the Hurwitz zeta function [14]

$$\zeta(q, m) = \frac{1}{q-1}m^{1-q} + \frac{1}{2}m^{-q} + 2m^{1-q} \int_0^\infty dx \frac{\sin(q \tan^{-1} x)}{(1+x^2)^{q/2}(e^{2\pi mx} - 1)}. \quad (\text{A1})$$

One can see that the integral is of order  $m^{-1}$  in the limit  $m \rightarrow \infty$  since

$$\begin{aligned} & \int_0^\infty dx \frac{\sin(q \tan^{-1} x)}{(1+x^2)^{q/2}(e^{2\pi mx} - 1)} \\ & \lesssim \int_0^{1/m} dx \frac{qx}{e^{2\pi mx} - 1} + \int_{1/m}^\infty dx \frac{1}{e^{2\pi mx} - 1} \\ & \simeq \mathcal{O}(m^{-2}) + \mathcal{O}(m^{-1}), \end{aligned} \quad (\text{A2})$$

and thus for  $0 < q < 1$ ,  $H_m^q$  behaves as

$$H_m^q = \sum_{k=1}^m \frac{1}{k^q} \simeq \frac{(m+1)^{1-q}}{1-q} + \zeta(q) + \mathcal{O}(m^{-q}). \quad (\text{A3})$$

When  $\eta > 0$ , the terms with such diverging coefficients exist and thus we can rearrange the expansion as follows:

$$\begin{aligned} \bar{r} &= \sum_{n=0}^\infty \frac{(n-1/2)!(-1)^n (J\bar{r})^{2n+1} H_{k_m}^{\lambda-\eta-2n\eta-1}}{2^{n+3/2} n! (n+1)! \zeta(\lambda-1)} \quad (\text{A4}) \\ &= \sum_{n=0}^\infty \frac{(n-1/2)!(-1)^n \zeta(\lambda-\eta-2\eta n-1)}{2^{n+3/2} n! (n+1)! \zeta(\lambda-1)} (J\bar{r})^{2n+1} \\ &\quad + \sum_{n=n_c}^\infty \frac{(n-1/2)!(-1)^n k_m^{2+\eta+2n\eta-\lambda} (J\bar{r})^{2n+1}}{2^{n+3/2} n! (n+1)! (2+\eta+2n\eta-\lambda) \zeta(\lambda-1)} \\ &= \sum_{n=0}^\infty \bar{B}_n (J\bar{r})^{2n+1} + (J\bar{r})^{(\lambda-2)/\eta} \bar{C}(J\bar{r} k_m^\eta), \end{aligned} \quad (\text{A5})$$

where we approximated  $H_{k_m}^{\lambda-1}$  by  $\zeta(\lambda-1)$  since  $\lambda-1 > 1$ . The coefficients  $\bar{B}_n$  are defined in Eq. (17) and the function  $\bar{C}(x)$  is defined by

$$\begin{aligned} \bar{C}(x) &= \sum_{n=n_c}^\infty \bar{c}_n x^{(2+\eta+2n\eta-\lambda)/\eta}, \quad \text{with} \\ \bar{c}_n &= \frac{(n-1/2)!(-1)^n}{2^{n+3/2} n! (n+1)! (2+\eta+2n\eta-\lambda) \zeta(\lambda-1)}. \end{aligned} \quad (\text{A6})$$

While  $\bar{C}(x)$  behaves as  $x^{(2+\eta-\lambda+2\eta n_c)/\eta}$  for  $x \ll 1$ , it converges to a constant  $\bar{C}_\infty$  for  $x \rightarrow \infty$  yielding a non-analytic term  $\bar{C}_\infty (J\bar{r})^{(\lambda-2)/\eta}$  as can be seen in Eq. (22).

Therefore, the magnitude of  $J\bar{r}k_m^\eta$  is essential for the determination of the leading behaviors of the right-hand-sides of Eqs. (15) and (16) for  $\bar{r} \ll 1$ . If  $J\bar{r}k_m^\eta \gg 1$ , one can approximate the function  $\bar{C}(J\bar{r}k_m^\eta)$  by a constant  $\bar{C}_\infty$  that is evaluated as

$$\begin{aligned} \bar{C}_\infty &= \lim_{x \rightarrow \infty} \sum_{n=n_c}^{\infty} \frac{(n-1/2)!(-1)^n 2^{-(\lambda+2\eta-2)/(2\eta)}}{n!(n+1)!(2+\eta+2n\eta-\lambda)\zeta(\lambda-1)} \\ &\quad \times (2^{-1/2}x)^{(2+\eta+2n\eta-\lambda)/\eta} \\ &= \frac{1}{2^{(\lambda+2\eta-2)/(2\eta)}\zeta(\lambda-1)} \sum_{n=n_c}^{\infty} \frac{(-1)^n (n-1/2)!}{n!(n+1)!} \\ &\quad \times \int_0^\infty dy y^{1+\eta+2n\eta-\lambda} \\ &= \frac{[(\lambda-2\eta-2)/2\eta]![(2-\lambda-\eta)/2\eta]!}{\eta 2^{(\lambda+4\eta-2)/2\eta} [(\lambda+\eta-2)/2\eta]!\zeta(\lambda-1)}. \quad (\text{A7}) \end{aligned}$$

The function  $C(x)$  defined in the text can be approximated in the same way by a constant  $C_\infty$  that is identical to  $\bar{C}_\infty$  with  $\lambda+1$  in place of  $\lambda$ . Therefore, one should refer to Eqs. (22) and (23) for the correct expansions of  $r$  and  $\bar{r}$  around  $\bar{r} = 0$  in the case of  $J\bar{r}k_m^\eta \gg 1$  while Eqs. (15) and (16) can be used in the case of  $J\bar{r}k_m^\eta \ll 1$ .

- 
- [1] A. S. Pikovsky, M. G. Rosenblum, and J. Kurths, *Synchronization—A Universal Concept in Nonlinear Sciences* (Cambridge University Press, Cambridge, 2001); S. Boccaletti, J. Kurths, G. Osipov, D. L. Valladares, and C. S. Zhou, *Phys. Rep.* **366**, 1 (2002).
- [2] D. J. Watts and S. H. Strogatz, *Nature* **393**, 440 (1998).
- [3] M. Barahona and L. M. Pecora, *Phys. Rev. Lett.* **89**, 054101 (2002).
- [4] A.-L. Barabási and R. Albert, *Science* **286**, 509 (1999).
- [5] T. Nishikawa, A. E. Motter, Y.-C. Lai, and F. C. Hoppensteadt, *Phys. Rev. Lett.* **91**, 014101 (2003).
- [6] A. E. Motter, C. Zhou, and J. Kruths, *Phys. Rev. E* **71**, 016116 (2005).
- [7] Y. Kuramoto *Chemical Oscillations, Waves and Turbulence* (Springer, Berlin, 1984); Y. Kuramoto, *Prog. Theor. Phys. Suppl.* **79**, 223 (1984).
- [8] T. Ichinomiya, *Phys. Rev. E* **70**, 026116 (2004).
- [9] D.-S. Lee, *Phys. Rev. E* **72**, 026208 (2005).
- [10] S. H. Strogatz, *Physica D* **143**, 1 (2000).
- [11] K.-I. Goh, B. Kahng, and D. Kim, *Phys. Rev. Lett.* **87**, 278701 (2001).
- [12] J. Garcia-Ojalvo and J. M. Sancho *Noise in Spatially Extended Systems* (Springer, New York, 1999).
- [13] D. Stauffer and A. Aharony, *Introduction to percolation theory* (Taylor & Francis, London, 1992).
- [14] D. Cvijovic and J. Klinowski, *Math. Comput.* **68**, 1623 (1999).
- [15] M.E. Fisher, S.-k. Ma, and B.G. Nickel, *Phys. Rev. Lett.* **29**, 917 (1972).
- [16] K.-I. Goh, D.-S. Lee, B. Kahng, and D. Kim, *Phys. Rev. Lett.* **91**, 148701 (2003); D.-S. Lee, K.-I. Goh, B. Kahng, and D. Kim, *J. Korean Phys. Soc.* **44**, 633 (2004); *Physica A* **338**, 84 (2004).